Chemistry–A European Journal
Research Article
doi.org/10.1002/chem.202400422
Chemistry Europe
European Chemical Societies Publishing
www.chemeurj.org

Steric Effects on Single-Molecule Conductance in Flat-Lying Phenanthrene

Kevin Batzinger,[a] Qinghai Zhou,[b] Xiang Ye,[c] Eric Borguet,[d] Shengxiong Xiao,[b] and Manuel Smeu*[a]

A previous combined experimental and theoretical study found that the position of anchoring groups on a phenanthrene (PHE) backbone played a large role in determining the single-molecule conductance of the PHE derivative. However, a consistent 0.1 G_0 feature was found across all PHE derivatives. To understand this, the previously investigated PHE derivatives were placed flat on a simulated Au substrate with a scanning tunneling microscope (STM) tip over PHE and conductance was calculated using the non-equilibrium Green's function technique in conjunction with density functional theory (NEGF-DFT). The location of the tip was varied to find the most conductive and most energetically favorable arrangements, which did not coincide. Furthermore, the variation in conductance found in erect junctions was not present when PHE derivatives were lying flat, with all derivatives calculated to have conductance values around 0.1 G_0.

Introduction

Molecular electronics is focused on the study of current flow at the fundamental size limit, allowing for key insight into how quantum behavior affects charge transport characteristics in mesoscopic systems.[1–5] Graphene-based organic molecules such as graphene nanoribbons (GNRs) provide the basic building blocks of molecular electronics and have high mechanical strength, stability, and carrier mobility, and are the basis for devices with applications in molecular rectification, switching, spin filtering, and field-effect devices.[5–14] Of particular interest is the effect investigating how different anchoring configurations on a common carbon backbone affect electron transport across the molecule. Previously, density functional theory (DFT) studies on polycyclic aromatic hydrocarbons (PAHs) have shown that acene derivatives have near length-independent conductance and that the anchoring configuration (steric effect) could dominate the conductance behavior.[15] However, extensive studies into how steric effects alter the single-molecule conductance of PAHs anchored between electrodes are limited to a few examples.[16] This led to an extensive theoretical and experimental study of the effects of anchoring group positions in the smallest armchair GNR (aGNR) unit, phenanthrene (PHE) by Chen *et al.*[16]

Chen *et al.* substituted SMe anchor groups onto different positions of a PHE backbone and measured the conductance via scanning tunneling microscopy-break junction (STM-BJ) experiments, complementing their findings with NEGF-DFT calculations. They found a hierarchy of conductances, with PHE with anchors in the 2,7 positions presenting the highest conductance, and the hierarchy of conductance values being $G_{2,7} > G_{3,6} > G_{2,6} > G_{1,7} > G_{1,6} > G_{1,8}$. However, a consistent bright spot in the 2-D conductance histograms occurred at 0.1 G_0 across all molecules, suggesting junction formation between the tip, Au (111) surface, and PHE derivatives prior to erect junction formation. This is in agreement with a dearth of literature reporting similar 0.1 G_0 features seen in experimental conditions and explained computationally.[17–24] The effect of molecule orientation has been explored previously in literature using molecules such as 7,7,8,8-tetracyanoquinodimethane (TCNQ). Yasini *et al.* investigated the effect of both denticity and orientation on the conductance of TCNQ molecules, finding that upright TCNQ with a lower denticity had the highest conductance value.[25]

To investigate the consistent 0.1 G_0 feature previously identified,[17] we performed calculations utilizing DFT and the non-equilibrium Green's function technique in conjunction with density functional theory (NEGF-DFT) in the Vienna *ab initio* Simulation Package (DFT), Virtual NanoLab-Atomistix Toolkit software package (NEGF-DFT) and NanoDCAL code (NEGF-DFT). We investigated the same six molecules used in the study by Chen *et al.* (1,6-, 1,7-, 1,8-, 2,6-, 2,7-, 3,6-PHE-2SMe), except that these molecules were relaxed in such a way that they remained flat on the surface of an Au (111) substrate and STM tips were

[a] K. Batzinger, M. Smeu
Department of Physics, Binghamton University,
Vestal, NY, USA
E-mail: msmeu@binghamton.edu
[b] Q. Zhou, S. Xiao
The Education Ministry Key Lab of Resource Chemistry, Joint International Research Laboratory of Resource Chemistry of Ministry of Education, Shanghai Key Laboratory of Rare Earth Functional Materials, Shanghai Frontiers Science Center of Biomimetic Catalysis, and College of Chemistry and Materials Science, Shanghai Normal University,
Shanghai 200234, China
[c] X. Ye
Mathematics and Science College, Shanghai Normal University,
Shanghai 200234, China
[d] E. Borguet
Department of Chemistry, Temple University,
Philadelphia, PA, USA

simulated to be above either an anchoring group or the carbon backbone of the PHE molecule. We found that the variation in conductance previously identified for different anchoring group positions does not hold up when the molecules are in a "flat" configuration, and that the conductance values are remarkably similar across all PHE derivatives in the flat configuration.

Results and Discussion

To identify arrangements where Au tip-flat PHE molecule binding is more energetically favorable, as well as arrangements where the conductance is likely to be highest, we employed the Au tip/PHE molecule/Au (111) surface setup shown in Figure 5 and varied the lateral position of the tip relative to the static Au (111) surface and 2,7-PHE-2SMe molecule. The most energetically favorable configuration was found when the tip was centered over the SMe groups of 2,7-PHE-2SMe; however, the highest conducting configuration was found when the tip was centered over the central ring of the PHE molecule, as shown in Figure 1. Surprisingly, the highest conductance does not coincide with the lowest energy configuration of the cell, something seldom reported in literature. We expect trends identified in the tip position over 2,7-PHE-2SMe to be similar for the other derivatives (1,6- 1,7- 1,8- 2,6- and 3,6-PHE-2SMe). Through these data, we were able to construct two distinct junction geometries for each PHE derivative: one in which the tip is centered over the S atom in an SMe anchoring group (corresponding to the lowest energy arrangement), and one in which the tip is centered over the central PHE ring (corresponding to the highest conductance arrangement).

In the previous study by Chen *et al.* the positions of the anchoring groups strongly affect the single-molecule conductance by a factor of almost 20 when the molecule is positioned upright between an Au (111) surface and a scanning tunneling microscope tip, as evidenced by both experimental data and theoretical predictions. However, a bright spot consistently occurs in the 2-D conductance histograms of all PHE molecules near 0.1 G_0.[16] The 0.1 G_0 feature occurs at a very low tip-surface separation distance across all molecules, indicating that if junction formation occurs, the molecule must be lying flat on the surface when this feature is measured. This is consistent with STM imaging and STM-BJ studies,[17] combined with NEGF-DFT calculations,[18,19,25] on a variety of molecules. To evaluate this, we re-interpret the experimental data for this flat molecule junction, focusing on the behavior observed at low tip separation distances consistent with the feature near 0.1 G_0. Combining this with NEGF-DFT calculations, we elucidate the effects anchoring group positions have on single-molecule conductance when the PHE molecules are lying flat on an Au (111) surface, and compare this to the previously identified effects identified for PHE molecules in the upright position.

1D conductance histograms were recorded for all PHE derivatives, as shown in Figure 2. The experimental conductance values shown in Table 1 were obtained *via* Lorentz fitting of the high conductance (blue curves) and low conductance (red curves) peaks in the 1D histograms. The high conductance peaks are attributed to the PHE molecule lying flat in the junction, while the low conductance peaks are attributed to the PHE molecule positioned upright in the junction.

Despite the difference in anchoring positions, all derivatives show similar conductance values when the tip is placed over either the central ring or the S atom of the SMe anchoring group, as shown in Table 1. Noticeably, the conductance derived from experimental values no longer follows the same trend that was identified for the PHE derivatives in the upright positions. Here, a trend of $G_{1,6} > G_{2,6} > G_{2,7} > G_{3,6} > G_{1,8} > G_{1,7}$ was identified from experimental data as opposed to the $G_{2,7} > G_{3,6} > G_{2,6} > G_{1,7} > G_{1,6} > G_{1,8}$ trend from previous work by Chen

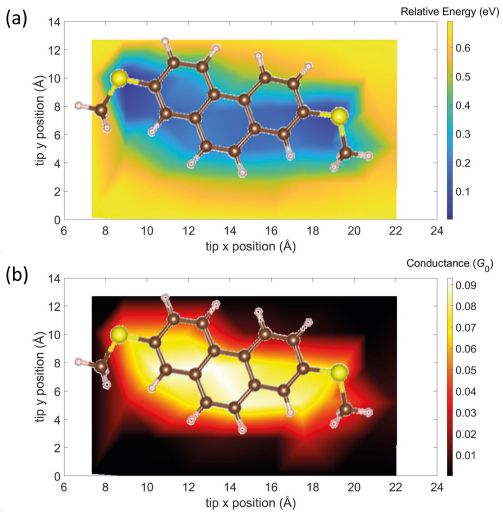

Figure 1. Color maps of the (a) relative energy and (b) conductance of the Au tip/2,7-PHE-2SMe/Au (111) surface simulation cell are shown as a function of tip *x*– and *y*– position. 2,7-PHE-2SMe is superimposed on the color maps to provide reference.

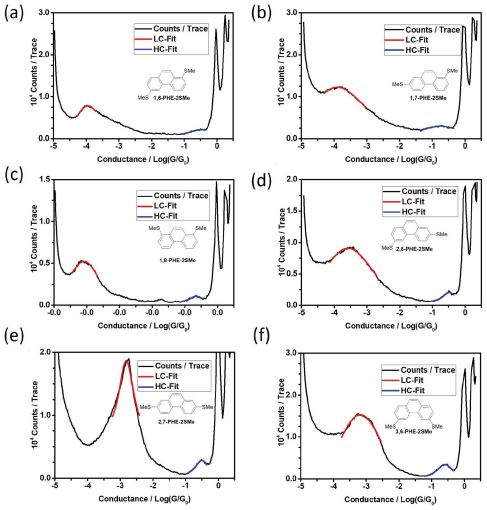

Figure 2. 1D conductance traces of (a) 1,6-, (b) 1,7-, (c) 1,8-, (d) 2,6-, (e) 2,7-, and (f) 3,6-PHE-2SME. The Lorentz fittings of high conductance (HC) peaks, shown in blue, represent conductance values obtained for the flat orientation of the PHE molecules. The Lorentz fittings of low conductance (LC) peaks represent the conductance values obtained for upright PHE molecules.

Table 1. Conductance values obtained in experiment and NEGF-DFT calculations. The upright and flat configurations are denoted by "(UR)" and "(FL)" respectively. The calc. PHE and calc. SMe headers refer to the configurations where the tip was positioned over the central PHE ring and SMe anchoring group, respectively.

	Conductance (G_0)				
PHE Derivative	exp. (UR)	calc. (UR)	exp. (FL)	calc. PHE (FL)	calc. SMe (FL)
1,6-PHE-2SMe	$1.02 \pm 0.72 \times 10^{-4}$	1.23×10^{-4}	$3.55 \pm 0.17 \times 10^{-1}$	8.32×10^{-2}	7.76×10^{-2}
1,7-PHE-2SMe	$1.32 \pm 1.18 \times 10^{-4}$	2.04×10^{-4}	$1.78 \pm 0.02 \times 10^{-1}$	8.51×10^{-2}	6.46×10^{-2}
1,8-PHE-2SMe	$8.13 \pm 3.74 \times 10^{-5}$	3.47×10^{-5}	$2.24 \pm 0.02 \times 10^{-1}$	7.59×10^{-2}	7.08×10^{-2}
2,6-PHE-2SMe	$2.63 \pm 1.60 \times 10^{-4}$	5.50×10^{-4}	$3.24 \pm 0.03 \times 10^{-1}$	8.91×10^{-2}	6.92×10^{-2}
2,7-PHE-2SMe	$1.51 \pm 0.02 \times 10^{-3}$	2.63×10^{-3}	$3.16 \pm 0.03 \times 10^{-1}$	1.12×10^{-1}	6.46×10^{-2}
3,6-PHE-2SMe	$6.61 \pm 4.62 \times 10^{-4}$	2.09×10^{-3}	$2.57 \pm 0.03 \times 10^{-1}$	9.12×10^{-2}	7.41×10^{-2}
Max *G*/Min *G*	18.62	75.86	1.74	1.48	1.20

et al.[16] The conductance hierarchy identified for the flat molecular junction in experiment does not agree with theoretical predictions, although in both theoretical predictions and experimental data the range of conductance values is much smaller than previously observed. In the upright configuration, conductance values varied by a factor of 18.62 in experiment and 75.86 in NEGF-DFT calculations.[16] For the flat configuration conductance values varied by a factor of 1.74 in experiment and 1.48 and 1.20 for NEGF-DFT calculations where the tip was over the central PHE ring or SMe groups, respectively.

The similarity in conductance values, whether the tip is positioned over the central PHE ring or an SMe anchoring group of a derivative, is especially borne out by the transmission spectra, as shown in Figure 3. Notably, all PHE derivatives have remarkably similar transmission function shapes and values around the Fermi energy of the Au electrode, despite having notably different transmission function behavior at energies far away (>1 eV) from the Fermi energy, with variations in transmission functions occurring at peaks nominally associated with the highest occupied (HOMO) and lowest unoccupied (LUMO) molecular orbitals of the derivatives. This suggests that transmission through the flat molecule at zero bias is not HOMO or LUMO mediated. This can be confirmed by plotting the transmission pathways for electrons between the Au tip, the PHE molecule, and the Au (111) surface, as shown in Figure 4.

Electron transmission pathways were calculated for the cases in which the tip was positioned over the SMe group of the PHE derivatives and also over the central PHE ring (Figure 4). In all cases, electrons tunnel directly from the tip, through the molecule and into the Au (111) surface, rather than traveling in molecular orbitals as occurs in the erect junction.[16] Combining this fact with the flat transmission spectra calculated around E_F, we conclude that electron transmission in this regime is not mediated by transmission resonances that occur in molecular orbitals such as the HOMO or LUMO, but rather occurs by direct tunneling from the tip to the surface through the molecule.

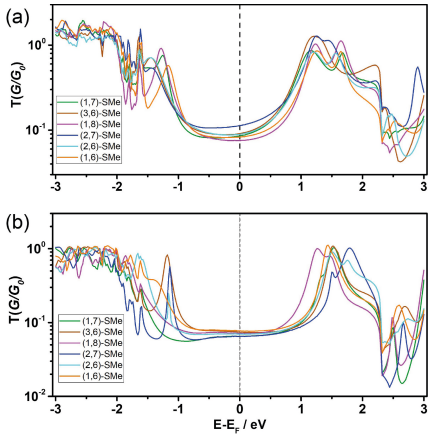

Figure 3. Transmission spectra are plotted for systems with (a) the Au tip over the PHE ring and (b) the Au tip over the SMe group of PHE derivatives.

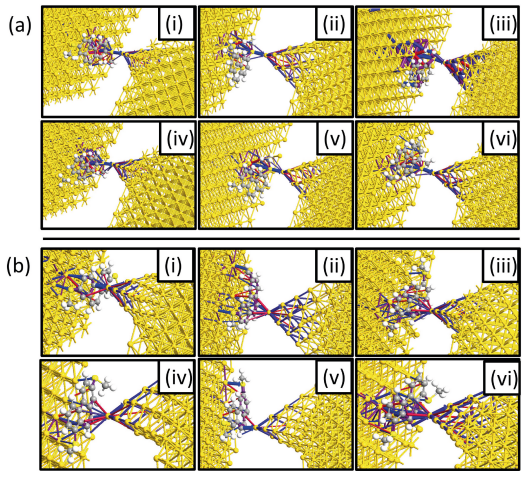

Figure 4. Transmission pathways are shown for (i) 2,7- (ii) 3,6- (iii) 1,6- (iv) 1,7- (v) 2,6- and (vi) 1,8- PHE-2SMe, where the tip is positioned over (a) the SMe group and (b) the central PHE ring of the derivatives.

Conclusions

Previously, the steric- and regio-effects of PHE were noted to have a conductance variation of almost 20 fold, but for each derivative, distinct features were noticed in the 2-D conductance histograms at 0.1 G_0 which suggested preliminary junction formation with the PHE derivatives lying flat on the surface. Follow-up DFT calculations were performed, and we found that the conductance variation identified for erect junctions did not hold up when the molecule was placed flat on the surface. Surprisingly, the most energetically favorable position for the tip and the most conductive arrangement of the tip/molecule/Au (111) simulation cell do not correlate, something seldom reported in literature. The conductance variation was much smaller for the flat-lying PHE molecules due to the fact that electrons tunnel directly through the molecule to the Au (111) surface, completely ignoring the molecular orbitals that are behind the conductance variation identified by Chen *et al.*[16] In fact, the lack of conductance variation and calculated conductance values, as well as correlation with experiment, support the idea that junction formation is behind the consistent feature identified around 0.1 G_0, shedding new light into processes that can be present in early-stage scanning-tunneling microscopy-break junction traces.

Methodology

Density Functional Theory

Structural relaxations were performed in the Vienna *ab initio* Simulation Package (VASP)[26] using a plane wave basis set and projector augmented wave (PAW) potentials[27] with the Perdew–Burke–Ernzerhof exchange-correlation functional (PBE),[28] the Γ *k*-point and a 400 eV plane-wave cutoff. Van der Waals forces were considered using the DFT-D3 method with Becke–Johnson damping.[29] The substrate was constructed from the Au (111) surface, and the PHE-derivatives were adsorbed onto the substrate. Subsequently, a tip was introduced to the simulation cell, and placed at a consistent distance of 5.85 Å above the substrate. To find the optimal position of the tip with regards to the PHE molecule, the tip position was varied in the *x-y* directions over 2,7-PHE-2SMe as shown in Figure 5, and the energy of each tip configuration was calculated. The most energetically favorable spot for the tip to interact with the molecule was calculated to be over the sulfur atoms of the -SMe anchoring groups (*vide supra*, Figure 1).

Non-equilibrium Green's Function-Density Functional Theory

NanoDCAL

In addition to identifying where the tip was most likely to bind to PHE molecules, preliminary conductance calculations were performed to identify where the Au tip/2,7-PHE-2SMe/Au (111) surface system exhibits the highest conductance using the code NanoDCAL.[30] The atomic cores were described by norm-conserving pseudopotentials and the valence electrons of the C, H, and S atoms in the PHE derivatives were described with a double-ζ polarized (DZP) basis set, while those of the Au atoms in the electrode were described with a single-ζ polarized (SZP) basis set.[31] The exchange-correlation functional adopted for this investigation was the Perdew-Burke-Ernzerhof approach in the generalized gradient aproximation (PBE-GGA).[28,32] Calculation of transport properties starts from the calculation of the Green's function of the system as a function of energy *E*,

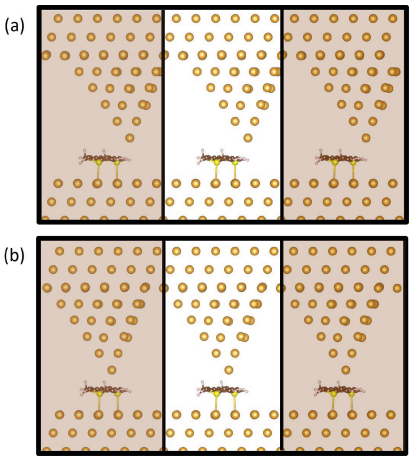

Figure 5. A side view of the Au tip/2,7-PHE-2SMe/Au (111) surface simulation cell, with the tip at the top of the images and the Au (111) substrate at the bottom. Two different tip positions which were placed in accordance with the lattice constants of Au (111) are shown in (a) and (b). The simulation cell is shown in the center of (a) and (b), with repeated images in the dark orange shaded images to the left and right.

$$G(E) = [(E + i\eta)S - H - \Sigma_1 - \Sigma_2]^{-1}. \quad (1)$$

In Eq. (1), *H* and *S* are the Hamiltonian and overlap matrices for the scattering region, respectively, η is a positive infinitesimal, and $\Sigma_{1,2}$ are the self-energies of the left and right electrodes.[30,33] The self-energies describe the effects of the coupling of the electrodes to the scattering region, and consist of both real and imaginary components. The real component represents a shift of the energy levels in the scattering region, and the imaginary component represents the broadening of these levels corresponding to the broadening matrix seen in Eq. (2),

$$\Gamma_{1,2} = i\left(\Sigma_{1,2} - \Sigma_{1,2}^{\dagger}\right). \quad (2)$$

The self-energy is calculated by an iterative technique.[34] The electronic density matrix is then obtained as,

$$\rho = \frac{1}{2\pi}\int_{-\infty}^{\infty}[f(E,\mu_1)G\Gamma_1 G^{\dagger} + f(E,\mu_2)G\Gamma_2 G^{\dagger}]\,dE, \quad (3)$$

where $\mu_{1,2}$ are the electrochemical potentials of the left and right electrodes and $f(E,\mu)$ is the Fermi-Dirac function which describes the occupation of an energy level given the energy and electrochemical potential, μ. With the Green's function obtained in Eq. (3), we can now obtain the transmission function $T(E)$ *via* Eq. (4), which gives the probability that an electron with a given energy *E* will transmit from one electrode through the scattering region into the other electrode as,[35]

$$T(E) = \mathrm{Tr}\left(\Gamma_1 G\Gamma_2 G^{\dagger}\right). \quad (4)$$

In the limit of zero applied bias, the value of the transmission function at the Fermi energy of the left electrode recovers the conductance of the system.[36] The highest conductance was calculated to occur when the tip was over the central ring of 2,7-PHE-2SMe. Subsequently, two arrangements were made for each molecule: one where the Au tip was over an SMe group of each PHE derivative, and one where the Au tip was centered over the central ring of each PHE derivative. These configurations were then used for the following NEGF-DFT calculations.

Atomistix

With the geometries from the above, single-molecule junctions were built to calculate the conductance and the electron transmission pathway *via* NEGF-DFT formalism as implemented in the Virtual NanoLab-Atomistix Toolkit (version 2015.1) software package in QuantumATK.[37,38] First, the central region consisting of the Au (111) surface, the PHE derivative, and the Au tip was joined with Au electrodes and relaxed for each derivative and binding geometry. Then, the conductance was calculated at the Perdew-Burke-Ernzerhof (PBE-GGA)[32,39] level implemented in ATK program with 1×1×200 *k*-point sampling. Calculation parameters included a mesh cut-off of 75 Hartrees and an electron temperature of 300 K. The density matrix was considered to be converged under a threshold of 10^{-4} Hartrees, and structural relaxations were performed until residual forces on all atoms were less than 0.05 eV/Å. In all ATK calculations, DZP (double-ζ polarized) basis sets were utilized for C, H, and S atoms while DZ (double-ζ) basis set for were employed for Au atoms.

Acknowledgements

K.B. and M.S. were supported by funds from Binghamton University. E.B. acknowledges the support of the National Science Foundation under grant CHE 2102557. S.X. and Q.Z. acknowledge financial support from NSFC under grant numbers 21772123, 21761142011, 51502173 and 21702095, the Shanghai Engineering Research Center of Green Energy Chemical Engineering under grant number 18DZ2254200, the "111" Innovation and Talent Recruitment Base on Photochemical and Energy Materials under grant D18020, the Shanghai Government under grants 21010503400 and 18JC1412900 and the International Joint Laboratory of Resource Chemistry (IJLRC).

Conflict of Interests

There are no conflicts of interest to declare.

Data Availability Statement

The data that support the findings of this study are available from the corresponding author upon reasonable request.

Keywords: electron tunneling · molecular electronics · orientation-dependent transport · scanning-tunneling microscope break-junction · steric effects

[1] A. Aviram, M. Ratner, *Chem. Phys. Lett.* **1974**, *29*, 277.
[2] A. Nitzan, M. Ratner, *Science* **2003**, *300*, 1384.
[3] J. Heath, M. Ratner, *Phys. Today* **2003**, *56*, 43.
[4] T. Su, M. Neupane, M. Steigerwald, L. Venkataraman, C. Nuckolls, *Nat. Rev. Mater.* **2016**, *1*, 16002.
[5] M. Smeu, O. Monti, D. McGrath, *Phys. Chem. Chem. Phys.* **2021**, *23*, 24106.
[6] A. H. Castro Neto, F. Guinea, N. M. R. Peres, K. S. Novoselov, A. K. Geim, *Rev. Mod. Phys.* **2009**, *81*, 109.
[7] A. Cresti, N. Nemec, B. Biel, G. Niebler, F. Triozon, G. Cuniberti, S. Roche, *Nano Res.* **2008**, *1*, 361.
[8] L.-L. Niu, H.-Y. Fu, Y.-Q. Suo, R. Liu, F. Sun, S.-S. Wang, G.-P. Zhang, C.-K. Wang, Z.-L. Li, *Phys. E: Low-Dimens. Syst. Nanostructures* **2021**, *128*, 11452.
[9] H. Wan, B. Zhou, X. Chen, C. Sun, G. Zhou, *J. Phys. Chem. C* **2012**, *116*, 2570.
[10] X. Liang, S. Wi, *ACS Nano* **2012**, *6*, 9700.
[11] A. Saraiva-Souza, M. Smeu, L. Zhang, A. G. Souza Filho, H. Guo, M. A. Ratner, *J. Am. Chem. Soc.* **2014**, *136*, 15065.
[12] A. Saraiva-Souza, M. Smeu, J. G. da Silva Filho, E. C. Girão, H. Guo, *J. Phys. Chem. C* **2018**, *122*, 15911.
[13] A. Saraiva-Souza, M. Smeu, J. G. da Silva Filho, E. C. Girão, H. Guo, *J. Mater. Chem. C* **2017**, *5*, 11856.
[14] A. Saraiva-Souza, M. Smeu, H. Guo, *Phys. Chem. Chem. Phys.* **2020**, *22*, 3653.
[15] J. Valdiviezo, P. Rocha, A. Polakovsky, J. L. Palma, *ACS Sens.* **2021**, *6*, 477.
[16] Y. Chen, M. Huang, Q. Zhou, Z. Li, J. Meng, M. Pan, X. Ye, T. Liu, S. Chang, S. Xiao, *Nano Lett.* **2021**, *21*, 10333.
[17] S. Afsari, Z. Li, E. Borguet, *Angew. Chem. Int. Ed.* **2014**, *53*, 9771.
[18] P. Yasini, S. Afsari, H. Peng, P. Pikma, J. Perdew, E. Borguet, *J. Am. Chem. Soc.* **2019**, *141*, 10109.
[19] S. Afsari, P. Yasini, H. Peng, J. Perdew, E. Borguet, *Angew. Chem. Int. Ed.* **2019**, *58*, 14275.
[20] M. Kiguchi, O. Tal, S. Wohlthat, F. Pauly, M. Krieger, D. Djukic, J. C. Cuevas, J. M. van Ruitenbeek, *Phys. Rev. Lett.* **2008**, *101*, 046801.
[21] Y. Komoto, S. Fujii, T. Nishino, M. Kiguchi, *Beilstein J. Nanotechnol.* **2015**, *6*, 2431.
[22] A. Martinez-Garcia, T. de Ara, L. Pastor-Amat, C. Untiedt, E. B. Lombardi, W. Dednam, C. Sabater, *J. Phys. Chem. C* **2023**, *127*, 23303.
[23] S. Kaneko, T. Nakazumi, M. Kiguchi, *J. Phys. Chem. Lett.* **2010**, *1*, 3520.
[24] S. Fujii, M. Iwane, S. Furukawa, T. Tada, T. Nishino, M. Saito, M. Kiguchi, *J. Phys. Chem. C* **2020**, *124*, 9261.
[25] P. Yasini, S. Shepard, T. Albrecht, M. Smeu, E. Borguet, *J. Phys. Chem. C* **2020**, *124*, 9460.
[26] G. Kresse, J. Furthmüller, *Phys. Rev. B* **1996**, *54*, 11169.
[27] P. Blöchl, *Phys. Rev. B* **1994**, *50*, 17953.
[28] J. Perdew, A. Ruzsinszky, O. Csonka, G. I. Vydrov, L. Scuseria, G. E. Constantin, X. Zhou, K. Burke, *Phys. Rev. Lett.* **2008**, *100*, 136406.
[29] S. Grimme, S. Ehrlich, L. Goerigk, *J. Comput. Chem.* **2011**, *32*, 1456.
[30] J. Taylor, H. Guo, J. Wang, *Phys. Rev. B* **2001**, *63*, 245407.
[31] N. Troullier, J. Martins, *Phys. Rev. B* **1991**, *43*, 1993.
[32] J. Perdew, K. Burke, M. Ernzerhof, *Phys. Rev. Lett.* **1996**, *77*, 3865.
[33] S. Datta, *Quantum Transport: Atom to Transistor*, Cambridge University Press, Cambridge, 1 edition **2005**.
[34] M. Lopez Sancho, J. Lopez Sancho, J. Rubio, *J. Phys. F* **1984**, *14*, 1205.
[35] M. Smeu, G. DiLabio, *J. Phys. Chem. C* **2010**, *115*, 17874.
[36] J. C. Cuevas, E. Scheer, *Molecular Electronics: An Introduction to Theory and Experiment*, World Scientific Series in Nanoscience and Nanotechnology, World Scientific Publishing Co. Pte. Ltd. **2017**.
[37] QuantumATK Synopsis.
[38] M. Brandbyge, J.-L. Mozos, P. Ordejón, J. Taylor, K. Stokbro, *Phys. Rev. B* **2002**, *65*, 165401.
[39] J. Perdew, K. Burke, M. Ernzerhof, *Phys. Rev. Lett.* **1997**, *78*, 1396.

Manuscript received: January 31, 2024
Accepted manuscript online: April 17, 2024
Version of record online: ■■, ■■

RESEARCH ARTICLE

Previous results identified a 20-fold difference in conductance between phenanthrene derivatives with different anchoring group positions when measured upright between a gold surface and STM tip. This variation disappears when the phenanthrene derivatives lie flat between the tip and gold surface, all derivatives exhibit a conductance around 0.1 G_0.

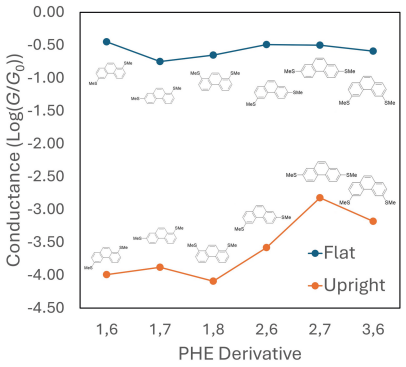

*K. Batzinger, Q. Zhou, X. Ye, E. Borguet, S. Xiao, M. Smeu**